JCTC Journal of Chemical Theory and Computation

Explaining Asymmetric Solvation of Pt(II) versus Pd(II) in Aqueous Solution Revealed by Ab Initio Molecular Dynamics Simulations

Elizabeth C. Beret,[†] José M. Martínez,[†] Rafael R. Pappalardo,[†] Enrique Sánchez Marcos,*[,†] Nikos L. Doltsinis,[‡,§] and Dominik Marx*[,‡]

Departamento de Quimica Fisica, Universidad de Sevilla, 41012 Sevilla, Spain, and Lehrstuhl für Theoretische Chemie, Ruhr—Universität Bochum, 44780 Bochum, Germany

Received January 8, 2008

Abstract: The solvation behavior of Pt(II) versus Pd(II) has been studied in ambient water using ab initio molecular dynamics. Beyond the well-defined square-planar first solvation shell encompassing four tightly bonded water molecules as predicted by ligand field theory, a second coordination shell containing about 10 H_2O is found in the equatorial region. Additional solvation in the axial regions is observed for both metals which is demonstrated to be induced by the condensed phase. For the Pt(II) aqua complex, however, this water molecule is bonded with one of its hydrogen atoms toward the cation, thus establishing a typical anionic solvation pattern, which is traced back to the electronic structure of Pt^{2+} versus Pd^{2+} cations, in particular to the anisotropic polarizability of their tetrahydrates. Systematic model calculations based on suitable aqua complex fragments embedded in a polarizable continuum solvent support the idea that anionic hydration is facilitated by the liquid. Furthermore, transient protolysis of water molecules in the first shell is observed for both divalent transition metal cations, being more pronounced for Pt(II) versus Pd(II). The relevance of these solvation features is discussed with respect to the different acidity of Pt^{2+} versus Pd^{2+} aqua ions in water, their different water ligand exchange rates, and force field modeling approaches.

1. Introduction

Metal-ion water solutions have received a large amount of attention from the scientific community during the last three decades. However, there is only scarce information available for Pd(II) and Pt(II) from experiment[1−5] and theory.[6−10] Nevertheless, their aqua ions are both well-known to form square-planar tetrahydrates,[11] which introduces a strong asymmetry in their hydration patterns. As a result, the "concentric shell model" of Frank and Evans[12] is no longer valid and thus cannot be used to understand the solvation structure in the nonequatorial regions. In this sense, although overall consensus between different experimental and theoretical investigations is achieved on the gross square-planar structure of these aqua ions, describing the axial regions above and below the metal-oxygen plane remains controversial. Previous EXAFS[3,4] and LAXS[3] studies on Pt(II) solutions depict a completely unpopulated axial region, while classical molecular dynamics (MD) simulations, employing interaction potentials obtained from first principles,[7,8] find a so-called "meso-shell". It consists of two labile water molecules axially coordinated to the metal cation, M^{2+}, at a M-O distance of about 2.67 and 2.95 Å for Pd(II) and Pt(II), respectively. A similar XAFS study on Pd(II) supports this picture,[5] while only one water molecule in the axial region is predicted from a QM/MM MD simulation of Pd(II) in ref 9. A more recent combined theoretical (QM/MM MD) and experimental (XAFS) study[10] reports, instead, the finding of two water molecules in the axial region of Pd(II), at

* Corresponding author e-mail: sanchez@us.es (E.S.M.) and dominik.marx@theochem.ruhr-unibochum.de (D.M.).

[†] Universidad de Sevilla.

[‡] Ruhr—Universität Bochum.

[§] Present address: Department of Physics, King's College London, Strand, London WC2R 2LS, United Kingdom.

10.1021/ct800010q CCC: $40.75
Published on Web 11/14/2008

2.7−2.8 Å from the metal, in agreement with the previous meso-shell picture.[7]

Previous analysis of X-ray scattering data on $PdCl_4^{2-}$ and $PtCl_4^{2-}$ showed two bonded water molecules at the apical sites of these square-planar ions, at a distance of 2.77 Å to the metal,[13] indicating a similar axial hydration pattern as that of the meso-shell obtained from classical MD.[7,8] However, in Monte Carlo[14] and Car-Parrinello MD[15] simulations of a solution of cisplatin (*cis*-$Pt(NH_3)_2(Cl)_2$) in water and in finite cluster solvation studies[16] no axial hydration structure such as the meso-shell was found at equilibrium, but apparently no further detailed analysis of coordination in the axial region was performed in those investigations. An analysis of the interaction energy between the $[Pt(NH_3)_4]^{2+}$ or *trans*-$[Pt(OH)_2(NH_3)_2]$ complex and a water molecule approaching the metal along the axial region in vacuum showed that a linear HO-H· · ·Pt arrangement, called "inverse hydration", is stabilized by electron dispersion contributions to bonding.[17,18] In particular, in the case of the cationic compound the interaction occurs preferentially via coordination through the oxygen atom, although "inverse hydration" is observed in terms of a metastable local minimum, while for the neutral compound an approach through the hydrogen atom is clearly favored.

Elucidation of the axial coordination pattern of Pd(II) and Pt(II) in aqueous solution not only is interesting from this fundamental physico-chemical point of view but also impacts onto biochemistry. Rate constants for water exchange at 298 K in these aqua ions are about 6 orders of magnitude higher for Pd(II) than for Pt(II), the difference being attributed to their corresponding activation enthalpies.[11] The exchange reaction is believed to follow an associative interchange mechanism[6] in which the transition state defines a trigonal bipyramid for a 5-fold hydrated cation. A similar behavior is observed for other Pd(II) and Pt(II) square-planar complexes including ligands such as H_2O, NH_3, or Cl^- when exchange of a water molecule takes place: the mechanism is associatively activated, and the reaction is faster for the Pd(II) case.[19,20] Some of these square-planar derivatives of Pt(II) such as cisplatin are reactive as anticancer drugs when they exchange their first-shell ligands for water molecules, while analogous coordination compounds of Pd(II) are not. The basis for this different behavior is thought to be the rate of ligand exchange, which happens too fast in the Pd(II) case to allow for the complex to reach its pharmacological target.[21] Thus, according to the water exchange mechanism, the axial hydration structure may play an important and discriminating role between Pd(II) and Pt(II) with respect to their pharmacological activities.

In the present study, Car-Parrinello molecular dynamics[22,23] (CP-MD) simulations for Pd(II) and Pt(II) in water at ambient conditions are presented, thus introducing dynamical nuclear and electronic degrees of freedom not considered in previous, classical MD simulations published by some of the authors.[7,8] The focus is on the hydration pattern in the axial versus equatorial regions beyond the first, square-planar hydration shell and, in particular, on the interplay of interactions defining them, thus going far beyond our preliminary short communication.[24] These dynamical condensed phase ab initio simulations in fully explicit solvent are complemented by ab initio calculations of finite, solvated tetrahydrate complexes within the Polarizable Continuum Model (PCM)[25−27] in order to disentangle the solvent effects on a qualitative level.

Furthermore, particular attention is paid to important changes in polarization and many-body effects that lead to transient protolysis of water molecules in the first coordination shell of the Pd(II) and Pt(II) tetrahydrates. Although proton transfer, autoprotolysis, and Grotthuss structural diffusion have been studied extensively in liquid water using the ab initio MD framework[28−32] as reviewed recently,[33] reports on ion-induced dissociation of water molecules as a source of proton transfer remain scarce. Temporary proton transfer events in aqueous solutions of *trivalent* Al(III) have been previously reported,[34,35] and even the 5-fold coordinated complex $[Al(H_2O)_4OH]^{2+}$ has been advocated as the predominant form of Al(III) in water under ambient conditions.[36] In addition, the mechanism and free energies of water dissociation induced by the *trivalent* transition metal cations Cr^{3+} and Fe^{3+} in aqueous solution has been revealed recently[37] using CP-MD. Since Al^{3+} features a distinctly different behavior, it has been concluded that "electrostatic effects alone do not fully account for water dissociation".[35] Here, we analyze quantitatively the electronic structure of the *divalent* transition metal Pd(II) and Pt(II) aqua complexes, and we gain additional insights into transient protolysis which is qualitatively related to experimental pK_a measurements.[1,2]

2. Methods

Ab initio molecular dynamics simulations within the Car-Parrinello approach,[22,23] CP-MD, have been performed of Pd(II) and Pt(II) cations in aqueous solution using the CPMD program package.[23,38] The PBE exchange and correlation GGA functional[39,40] was employed together with ultrasoft pseudopotentials[41] in conjunction with a plane wave basis set truncated at 30 Ry. Each system was set up to contain one metal dication and 70 water molecules in a periodically repeated cubic simulation box of length 13.140 Å and 13.418 Å for Pd and Pt, respectively, in order to reproduce the density of water at ambient conditions. Nose-Hoover chain thermostats were applied to both nuclei and electrons. The temperature was kept at 350 K in order to approximately correct for the underestimation of temperature using GGA-type functionals[42] thereby emulating room temperature, ≈300 K. The equations of motion were integrated using a time step of 4 au together with a fictitious electron mass parameter of 400 au and the hydrogen mass for H.

The starting configurations were taken from previous classical MD runs performed with Pd and Pt-water interaction potentials based on ab initio parametrization.[7,8] A 2 ps thermalization plus a 2 ps system relaxation period preceded each production run of over 11 ps length. The system configuration was saved every 10 MD steps (≈ 0.97 fs) for further analysis. For electronic structure analysis norm-conserving dual-space Gaussian pseudopotentials[43] and a plane wave cutoff of 80 Ry were employed.

The dynamical liquid phase simulations were supplemented by static gas phase electronic structure calculations

using finite solvation complexes subject to both vacuum conditions and the solvent effects induced by a continuum solvation model. Plane wave PBE gas phase calculations with the CPMD code were performed by applying cluster boundary conditions[23] to avoid spurious electrostatic coupling of periodic images of the charged clusters. In addition, PBE and MP2 gas phase calculations using Gaussian basis sets were carried out. For these calculations energy-consistent pseudopotentials from the Stuttgart/Köln group (ECP28MWB for Pd and ECP60MWB for Pt) and their corresponding optimized valence basis sets (cc-pVDZ type) for Pd and Pt[44] were used within the Gaussian03 package,[45] together with aug-cc-pVDZ basis sets[46] for O and H. The continuum calculations were used to study solvation complexes systematically as a function of a reaction coordinate describing hydration in the axial region and were carried out with the Polarizable Continuum Model (PCM)[25,27] in its Integral Equation Formalism (IEFPCM)[47−50] as implemented in the Gaussian03 package.[47] The dielectric continuum was chosen to represent liquid bulk water at 298 K, i.e. $\varepsilon = 78.39$. The cavities employed here were built by using atomic radii from the Universal Force Field[51] scaled by an alpha factor of 1.2 (r_{Pd}: 1.450 Å, r_H: 1.443 Å), and all hydrogen atoms were explicitly considered in the cavity definition.

The polarizabilities of the tetrahydrates in the gas phase were computed using the Gaussian03 package[45] with the PBE exchange and correlation functional. The tetrahydrate geometry was first optimized using the chosen electronic structure method. It has been reported that good values of polarizabilities of metal cations can be computed within the density functional framework if triple-zeta quality basis sets extended with diffuse and polarization functions are employed.[51] For the $[Pd(H_2O)_4]^{2+}$ case, two different pseudopotentials from the Stuttgart/Köln group, together with the corresponding optimized valence basis sets, were tested. The ECP28MWB pseudopotential with cc-pVDZ quality basis sets for Pd(II)[44] together with aug-cc-pVDZ basis sets[46] for O and H yields virtually identical results as the ECP28MDF pseudopotential with aug-cc-pVTZ-PP basis sets for Pd(II)[53] and aug-cc-pVTZ basis sets[46] for O and H. For Pt(II) no triple-zeta quality basis set from the Stuttgart/Köln group is available, so the ECP60MWB pseudopotential with cc-pVDZ quality basis set[44] was employed for this metal cation, together with aug-cc-pVDZ basis sets[43] for O and H.

3. Results

3.1. General Hydration Pattern. *3.1.1. Radial Distribution Functions.* The spherically averaged solvation structure around the Pd and Pt cations is first analyzed in terms of the usual metal-oxygen and metal-hydrogen radial distribution functions (RDFs) shown in Figure 1. The positions of the peak maxima r_M and the coordination numbers n are gathered in Table 1. The first solvation shell is sharply defined and integrates up to exactly four water molecules in both cases. Zero density in the RDFs after this M-O peak means that these four H_2O molecules remain in the first solvation shell during the whole simulation, as expected from previous data on mean residence times of H_2O in the closest environment

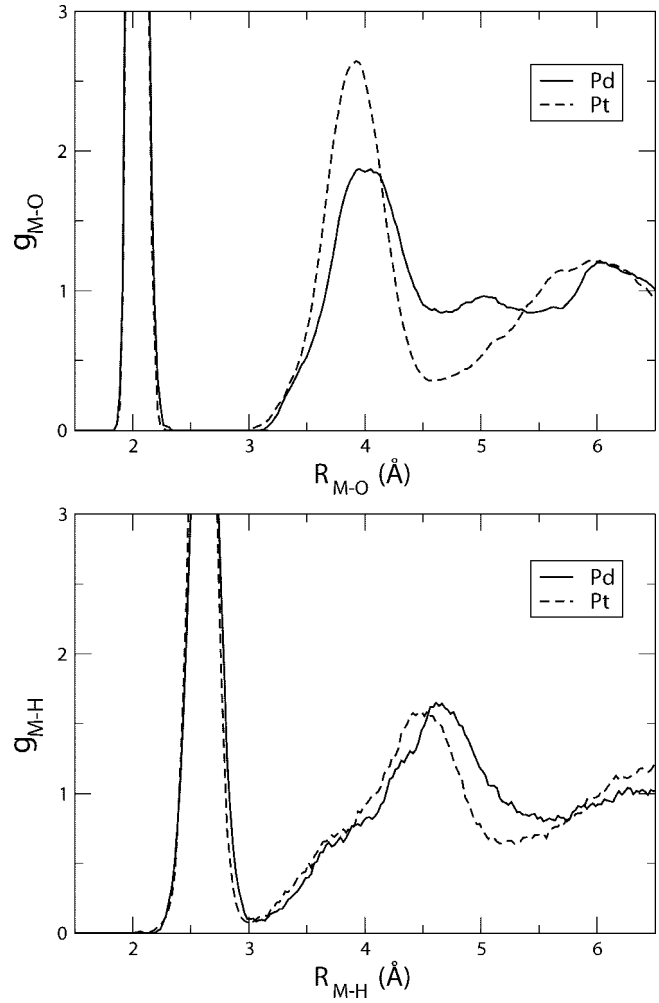

Figure 1. M-O and M-H radial distribution functions for aqueous Pd(II) (solid line) and Pt(II) (dashed line) solutions.

Table 1. Peak Maxima (r_M in Å), Coordination Numbers (n), and Underlying Integration Ranges (r_L in Å) from M-O and M-H Radial Distribution Functions of Aqueous Pd(II) and Pt(II) Solutions

	1st shell			2nd shell		
	r_M	n	r_L	r_M	n	r_L
Pd−O	2.04	4.0	0−2.31	4.02	10.3	2.31−4.64
Pd−H	2.61	8.0	0−3.10	4.64	37.1	3.10−5.56
Pt−O	2.04	4.0	0−2.26	3.91	9.9	2.26−4.56
Pt−H	2.61	8.6	0−3.10	4.50	26.2	3.10−5.19

of these cations.[19] The first M-O maximum appears at 2.04 Å for both Pd and Pt which is consistent with previous experimental and theoretically obtained values ranging from 2.00 to 2.07 Å, see refs 3−5 and 7−9. The corresponding M-H maxima are found at 2.61 Å which can be compared to a value of ≈2.7 Å found previously using classical MD simulations employing interaction potentials[7,8] based on MP2 calculations and also by QM/MM MD simulations at the Hartree-Fock level.[9,10]

The second hydration shell peaks are also clearly defined but quite different in Pd and Pt as the peak is higher and narrower in the case of Pt. In addition, a clear minimum appears after the second Pt−O peak, whereas this is absent

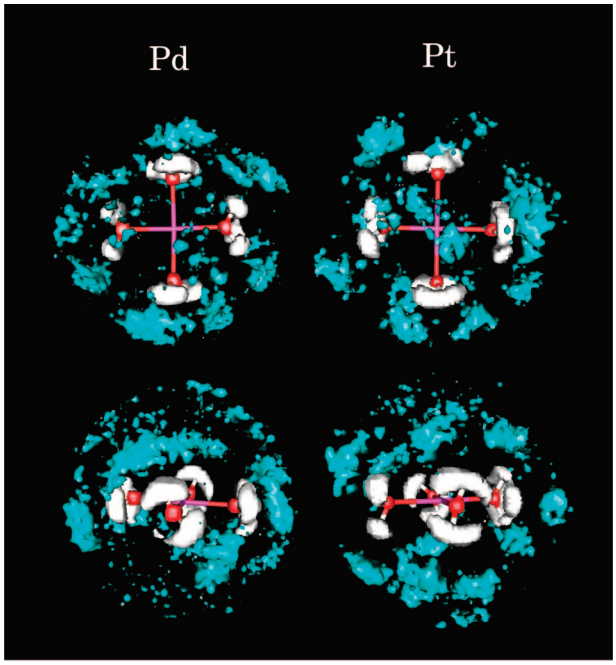

Figure 2. Spatial distribution functions for hydrogen atoms in the first solvation shell (white surfaces) and oxygen atoms in the first and in the second solvation shells (red and cyan surfaces, respectively) of Pd(II) and Pt(II), from apical (up) and equatorial (below) points of view. The average square-planar geometry of the tetrahydrates is represented as pink, red, and white bars.

in the Pd−O RDF. Thus the second solvation shell is more pronounced in the case of Pt compared to Pd. The second M-O peaks have maxima at 4.02 and 3.91 Å for Pd and Pt, respectively. These distances are shorter than those obtained from previous, classical MD simulations[7,8] (4.08 Å for both cations) and QM/MM MD simulations of Pd(II) (4.50 Å in ref 9 and 4.40 Å in ref 10) and integrate up to about 10 H_2O molecules.

3.1.2. Spatial Distribution Functions. The M-O and M-H RDFs merely provide spherically averaged information about the distribution of water molecules in the solution around the metal cation. Even though this purely radial information is of great value in itself, it is not sufficient when studying systems whose symmetry is clearly not spherical as in the present case. Here, spatial distribution functions (SDFs) presented in Figure 2 offer three-dimensional views of the solvation neighborhood around the metal cations.

The spatial picture obtained for Pd(II) and Pt(II) solutions is that of a well-defined square-planar first solvation shell, see Figure 2, allowing for the definition of an average plane containing the metal cation and those four oxygen atoms of H_2O that directly coordinate to the metal. The average orientation of the hydrogen atoms in these first-shell water molecules is distinctly different in Pd(II) and Pt(II) solution. In the Pd(II) case, the molecular plane of two H_2O are co-planar with the metal-oxygen plane, while the other two H_2O are perpendicular to it. For the Pt(II) tetrahydrate on the other hand none of the eight hydrogen atoms are contained in the metal-oxygen plane.

Most interesting is the behavior beyond the first solvation shell where a dense toroidal-shaped second hydration shell is observed to enclose the tetrahydrate cores. In stark contrast to the equatorial region, the axial regions remain sparsely populated. Still, some H_2O density is observed there at second-shell distances. However, these H_2O molecules are not strictly second-shell molecules, as they are not bonded to H_2O in the first hydration shell. Based on this qualitative knowledge a more quantitative analysis can be performed by using angle-resolved RDFs that focus onto the axial and equatorial solvation regimes.

3.1.3. Angular Decomposition of RDFs. The solvation space around the metal cations is split into different regions, which are defined by an azimuthal angle θ relative to the axis perpendicular to the average molecular plane of the tetrahydrate around the metal center. Then the RDFs for the molecules included in each of these regions can be obtained separately. Let us consider two hypothetical compounds, one with an octahedral arrangement of the oxygen atoms, O, around the metal center, M, and the other one with an hexagonal-planar structure according to the sketch in Figure 3. If all M-O average distances oscillate around one R_{MO} equilibrium value, both compounds will yield identical M-O *global* RDFs, their corresponding peaks centered at R_{MO} with a half-width of σ_{M-O} due to molecular vibrations. In order to distinguish between the two qualitatively different coordination structures, one can define a molecular plane and formally split the two hemispheres above and below into regions defined by the solid angle with respect to the axis normal to the molecular plane. The revolution of the generatrix line around this axis defines symmetric conical and semi-crown-shaped regions above and below the molecular plane. Then angle-resolved RDFs can be computed taking into account those molecules that are contained in each of those regions. To this aim, a reference *homogeneous* density ρ_{ref} is defined as the total number of O atoms in the simulation box divided by the total box volume V, as in a standard RDF computation. For each angular region the partial RDF, $g_p(r)$, is obtained by dividing the current oxygen density number (number of O atoms in a fraction of volume centered in r within the given angular region) by the reference density, ρ_{ref}. An application of this definition is shown in Figure 3, for the model example of two hexacoordinated metal compounds, MO_6, with the same average distance, R_{M-O}, but two different spatial distributions of O ligands around the metal M (octahedral and hexagonal-planar). Let us define two regions by means of the azimuthal angle: $\theta \in [0, 60]°$ and $\theta \in [60, 90]°$ where the two hemispheres, above and below the molecular plane, are considered to be equivalent due to symmetry. Each of these regions has a volume equal to half the total volume, $V_{[0,60]°} = V_{[60,90]°} = V/2$. The global RDFs show peaks of intensity $(6)/(\rho_{ref}V)$, and thus no distinction is observed between the octahedral and hexagonal-planar MO_6 compounds. However, when we compute angle-resolved RDFs, in the octahedral case peaks of intensities $(4)/(\rho_{ref}V)$ and $(8)/(\rho_{ref}V)$ are observed for the [0, 60]° and [60, 90]° regions, respectively. On the other hand, for the planar compound no signal is observed in the [0, 60]° region, while a peak of intensity $(12)/(\rho_{ref}V)$ appears in the [60, 90]° region. Thus, this type of decomposition of global RDFs into angle-resolved RDFs

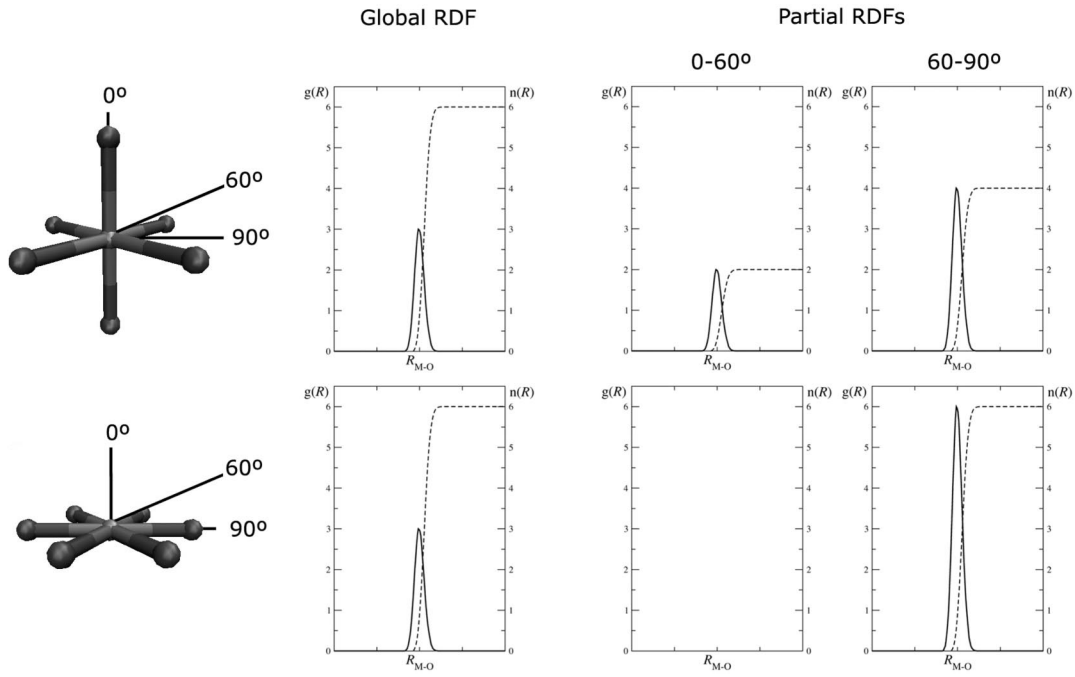

Figure 3. Decomposition of M-O global RDFs (left) into contributions coming from different angular regions for an octahedral (top) and a hexagonal-planar (bottom) MO_6 compound, see text for further details. RDFs and running integration numbers are represented by solid and dashed lines, respectively.

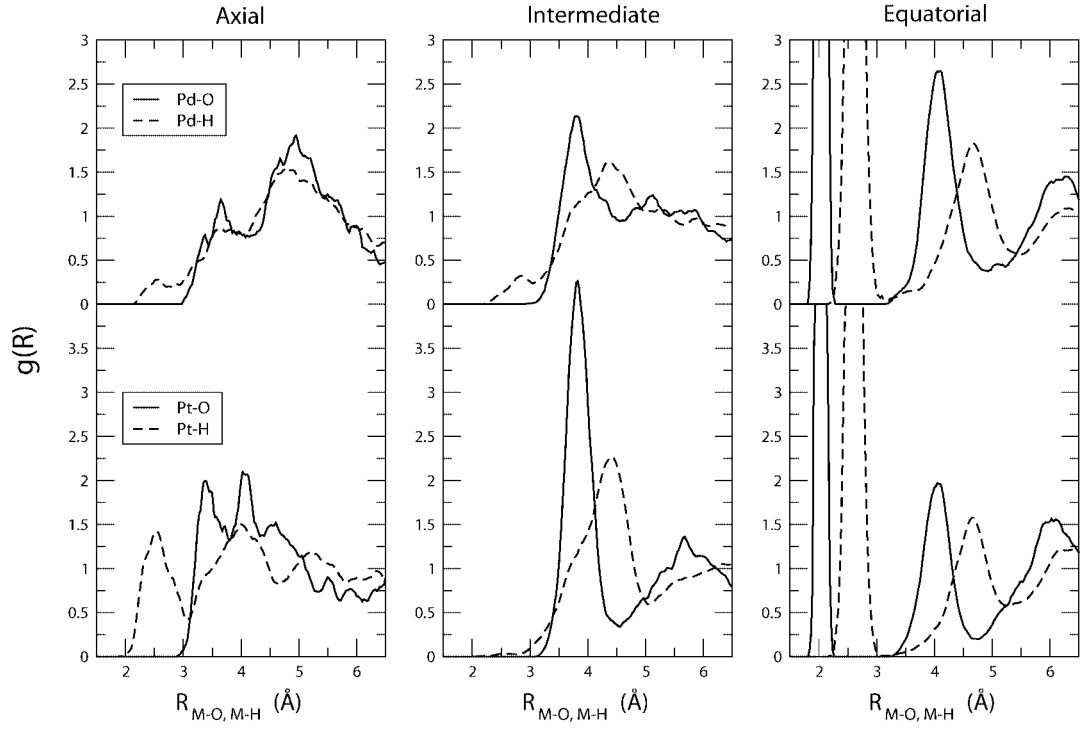

Figure 4. Decomposition of M-O (solid line) and M-H (dashed line) global RDFs for aqueous Pd(II) (top) and Pt(II) (bottom) solutions into three angular regions defined by the solid angle θ defined in Figure 3: axial region: $\theta \in [0, 30]°$, intermediate region: $\theta \in [30, 60]°$, and equatorial region: $\theta \in [60, 90]°$.

helps to extract a quantitative understanding from the distribution of ligands around a given metal center.

In the case of the Pd(II) and Pt(II) tetrahydrates with a square-planar first solvation shell, three angular regions were defined within the angular ranges $\theta \in [0, 30]°$ (termed *axial* region), $\theta \in [30, 60]°$ (*intermediate* region), and $\theta \in [60, 90]°$ (*equatorial* region). For each configuration snapshot selected for this analysis all water molecules were uniquely assigned to one of the three regions. Figure 4 depicts the resulting angular decomposition of the global M-O and M-H RDFs for the Pd(II) and Pt(II) aqueous solutions. In these angle-resolved RDFs one can clearly observe that the closest water molecules appear in the equatorial region, which is quite similar for both

Table 2. Reconstruction of the Second Hydration Shell in Aqueous Pd(II) and Pt(II) Solutions Based on the Different Contributions in Terms of Angle-Resolved RDFs Introduced in Figure 4[a]

	r_L	[0,30]°	[30,60]°	[60,90]°	n
Pd−O	2.31−4.64	1.0	4.0	5.3	10.3
Pt−O	2.26−4.56	1.7	4.6	3.6	9.9

[a] [0, 30]°, [30, 60]°, and [60, 90]° label the integration numbers obtained for the angle-resolved RDFs within the reported r_L integration limits (in Å) corresponding to axial, intermediate, and equatorial regions, respectively, and n is the sum of the three angle-resolved contributions.

Pd and Pt solutions. It includes peaks from the first hydration shell, in accordance with the average square-planar geometry of the tetrahydrates as well as part of the second hydration shell. Furthermore, the Pt−H RDF also features a pronounced peak at short distances which is not observed for the Pd case.

Remarkable differences between the two systems can be found in the intermediate and axial regions. The second solvation shell is mainly distributed among the [30, 60]° and [60, 90]° regions. The differences between Pd(II) and Pt(II) second shells are more clearly observed in these partial RDFs than in the global RDFs. In the case of Pt(II), a strong M-O peak appears in the [30, 60]° region, and smaller contributions are found in the axial (peak centered at ≈4 Å) and equatorial regions. For Pd(II) the second hydration shell is more evenly distributed among the [30, 60]° and [60, 90]° regions. These different distributions of the second solvation shell can be understood taking into account the average orientations of the hydrogen atoms in the first solvation shell observed in the SDFs (see Figure 2). In the Pt(II) case, most hydrogen atoms are located above and below the metal−oxygen plane, therefore forcing the second-shell H_2O molecules, which are directly bonded to them, to be further away from the metal-oxygen plane than in the Pd(II) case.

In the axial region a maximum at 2.55 Å can be found in the Pt−H RDF which integrates to 0.6 hydrogen atoms. A corresponding Pt−O peak can be found at around 3.50 Å integrating also to 0.6 oxygen atoms. These two peaks are evidence for a water molecule that is weakly bonded to the metal cation through a hydrogen atom, i.e. this water molecule is oriented as if it was coordinated to an anion. Therefore this coordination pattern may be termed *anionic hydration*. A second Pt−O peak at 4 Å is observed, integrating up to 0.8 oxygen atoms, which represents a second H_2O molecule in the axial region but at a second-shell distance and bonded through the oxygen atom. In the Pd(II) case the Pd−H peak can also be found, but it is much less defined. There is only one Pd−O peak around 3.5 Å (close to second-shell distances) which integrates up to 1.1 oxygen atoms. For Pd the axial water molecule is poorly oriented, its interaction with the Pd(II) cation being much weaker than in the Pt(II) case and being established through the oxygen atom. It is worth noticing that particular structural features hardly visible in the global RDFs are clearly observed by means of constructing these partial RDFs.

In Table 2 the number of water molecules contributing to the second peaks found in the global RDFs are reconstructed based on the contributions from the angle-resolved RDFs. Putting together all the structural information so far obtained, the solvation pattern of Pd(II) and Pt(II) can be described as follows. For both cations the first hydration shell is well defined and composed of four water molecules arranged in an average plane defined by the metal cation and the four first-shell oxygen atoms. At typical second hydration shell distances about 10 H_2O are found, which are mainly located in the *equatorial region* thereby enclosing the square-planar aqua ions in a crownlike arrangement. Eight of them are directly bonded to the four H_2O molecules in the first hydration shell, thus constituting a proper second hydration shell. In the Pt(II) case, the two additional H_2O molecules are disposed in the axial region, their orientations being anionic for one of them and through the oxygen atom for the other one as shown in Figure 5 using a representative configuration. However, their residence time in the axial region is rather short, indicating a weak interaction with the metal cation. For Pd(II), only one H_2O molecule enters the axial region, interacting with the metal through the oxygen atom and residing for a shorter time than in the Pt(II) case, whereas the other water molecule is a *bridge* H_2O, which helps to strengthen the structure within the second hydration shell (see Figure 5).

Although the overall solvation scenario in terms of a rigid square-planar first solvation shell and a less defined second shell is in agreement with other theoretical[6−10] and experimental[1−5] investigations, the previously found axial hydration structures for Pd(II) and Pt(II) were quite different. In classical MD simulations[7,8] a pronounced meso-shell consisting of two H_2O molecules bonded to the metal cation through their oxygen atoms was found for both Pd(II) and Pt(II). These axial H_2O showed a much higher persistence than in ab initio MD and were located at a distance of 2.67 and 2.95 Å from the metal for Pd(II) and Pt(II), respectively, in agreement with XAFS experimental results.[5] A similar orientation was found within the QM/MM simulation framework[9,10] for one or two tighter H_2O molecules in the axial region of Pd at a distance of 2.5−2.8 Å from the metal cation. However, the possibility of square-planar compounds of Pt(II) accepting coordination from an axial water molecule through its hydrogen atom (referred to as "inverse hydration") was already suggested for the case of the neutral microsolvated *trans*-$[Pt(OH)_2(NH_3)_2]$. H_2O complex in vacuume.[17,18]

When dealing with cations in aqueous solution, a perfect, collinear ion-dipole orientation of solvation water with respect to the metal cation would be characterized by a tilt angle of 180° (being the angle between the geometric dipole moment vector of the bonded H_2O molecule and the vector between the cation and the oxygen atom of this molecule). However, already the pioneering classical MD study of an electrolyte solution[54] observed a significant tilt which is consistent with an arrangement where one of the lone pairs rather than the dipole vector points toward the cationic center. This picture has been confirmed by subsequent simulations as well as by diffraction experiments.[55] In the current CP-MD simulations the first shell water molecules show an average tilt angle of ca. 135° and 132° for Pd(II) and Pt(II), respectively, to be compared with ≈165° for both Pd(II) and

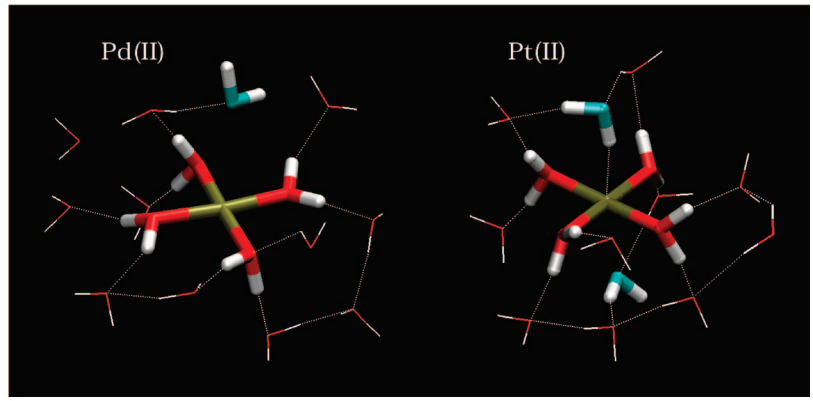

Figure 5. Snapshots sampled from the simulations of aqueous Pd(II) and Pt(II) solutions showing the tetrahydrate cores (licorice representation with red oxygen atoms), water molecules in the axial region (licorice representation with blue oxygen atoms), and some second shell and bulk water molecules; hydrogen bonds are sketched as dotted white lines.

Pt(II) obtained from classical MD and ≈175° in the above-mentioned Pd(II) QM/MM simulations. When the axial H_2O molecule comes close to the cation, its average tilt angle decreases to ≈100° for Pd(II) in the present CP-MD simulation to be compared to ≈100° and 90° in the above-cited classical MD and QM/MM MD approaches, respectively. An "anti ion-dipole" orientation with a tilt angle close to 0° would represent the other limiting behavior. On the other hand, the typical solvation of anions such as Cl^- as the prototype occurs preferentially via the hydrogen atoms of the first shell H_2O molecules yielding a tilt angle of typically 50 ± 10°, see refs 54 and 55. These angles should be compared to an average tilt angle of ≈40° observed in the CP-MD simulation for the axial water molecules around Pt(II). Clearly, the orientation of these axial water molecules with respect to the cation cannot be classified as a typical cationic solvation pattern, whereas it fits rather well the anionic hydration scenario. In the following, this peculiar solvation beyond the square-planar first shell will be dissected.

3.2. Axial Hydration. At first glance, the hydration of Pd(II) and Pt(II) aqua ions in the axial regions above or below the square plane, although dynamical and scarce, seems striking for various reasons. First of all, standard ligand field theory predicts a square-planar 4-fold coordination to be the most stable situation for these aqua ions leaving the axial regions as completely void spaces between the tetrahydrate and the bulk. Second, the hydration pattern in the axial region is very different between these two tetrahydrates, despite the similarities found in the intermediate and equatorial regions. In the Pd(II) case, one H_2O slightly escapes the second solvation shell, entering the axial region oriented toward the metal cation through the oxygen atom. For Pt(II), in contrast, one of the axial H_2O approaches the metal cation not through the oxygen atom, as expected, but through the hydrogen atom like in an anionic solvation shell. In order to gain further insights into these surprising results two different procedures have been employed: analysis of the electronic structure and description of interaction energies in gas phase and in solution.

3.2.1. Electronic Structure Analysis. Random snapshots were sampled from the simulation trajectory of Pt^{2+} in aqueous solution. The system was conceptually separated into the following components: the tetrahydrate $[Pt(H_2O)_4]^{2+}$, the axial H_2O molecule with anionic orientation, a second-shell H_2O molecule, and the remaining solvent. The electronic (valence) density and the total electrostatic potential were computed for each of these entities which were subtracted from the functions corresponding to the whole system. This strategy allows for a comparison of the axial interaction with a standard hydrogen bond between a water molecule in the first solvation shell of Pt and a second-shell H_2O molecule.

This analysis shows that there is a certain charge transfer from the axial water molecule and the metal cation toward the region between them, as seen by a net displacement of the electronic density toward that region (white lobe) in the left panel of Figure 6a. In addition, the relative electrostatic potential is observed to become more negative, i.e. less electron attracting, in that region depicted by the red area in the right panel of Figure 6a. This pattern is qualitatively similar to the hydrogen bond between the first and second solvation shells observed for the same snapshot (see Figure 6b) The main effect of the interaction is the increase of electronic density (or negative charge character) in the region between the atoms involved, revealed by a pronounced white lobe in that region of space concurrent to a more negative relative electrostatic potential (red area). Therefore this anionic interaction behaves like a weak hydrogen bond formed between the hydrogen atom of the axial H_2O molecule and the polarized Pt(II) cation. This interpretation is reinforced by an additional analysis in terms of maximally localized Wannier functions.[56] When anionic axial hydration is established, the Wannier center located along the Pt−H direction moves slightly away from the Pt ion toward the hydrogen atom of the axial H_2O molecule, enlarging the average metal to Wannier center distance of 0.38 Å to 0.44 Å signaling polarization. In addition, we have computed Kohn-Sham canonical orbitals for a snapshot extracted from the Pt(II) simulation in which anionic hydration takes place. The resulting orbitals indicate an interaction between the $5d_{z^2}$, $5d_{xz}$, and $5d_{yz}$ orbitals of the metal and orbitals of the axial water molecule, the contribution of the $5d_{z^2}$ being more important than that of the $5d_{xz}$ and $5d_{yz}$ orbitals.

In solution, the more pronounced localization of the solvent electronic density in the equatorial region induces a

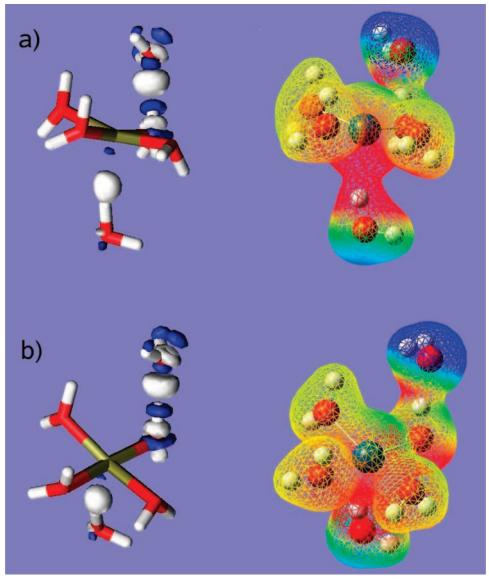

Figure 6. Electronic structure analysis of the anionic hydration of the solvated Pt(II) tetrahydrate compared to a proper hydrogen bond between a first-shell and a second-shell water molecule. A representative snapshot is shown in two orientations revealing the axial (a) and equatorial (b) interactions. Left: Electronic (valence) density difference (see text) shown by isosurfaces at +0.005|*e*| (white lobe) and −0.005|*e*| (blue lobe). Right: Electronic (valence) density surface (isosurface at +0.02|*e*|) onto which the change in electrostatic potential (see text) is mapped ranging from −0.02 au (red) via yellow and green to +0.02 au (blue).

Table 3. Isotropic Polarizability, α_{iso}, and Anisotropic Components, $\alpha_{xx} = \alpha_{yy}$ and α_{zz}, in au^3 Computed for the Pd(II) and Pt(II) Tetrahydrates in Vacuum[a]

complex	basis set	α_{iso}	$\alpha_{xx} = \alpha_{yy}$	α_{zz}
$[Pd(H_2O)_4]^{2+}$	ECP28MWB	52.2	58.7	39.2
	ECP28MDF	52.3	58.7	39.6
$[Pt(H_2O)_4]^{2+}$	ECP60MWB	53.7	58.8	43.6

[a] The square-planar tetrahydrate lies in the *xy* plane and *z* is the axial direction. The basis sets are labeled according to the pseudopotential chosen for the metal cation (see section 2 Methods).

slight electronic density redistribution of the metal, where the more diffuse character of the d_{z^2} orbital occupying the axial region stabilizes the system. In the case of the Pt(II) tetrahydrate this delocalization is sufficient for a dynamic anionic arrangement with a single H_2O molecule to take place. In the Pd(II) species the $4d_{z^2}$ orbital is less diffuse than the $5d_{z^2}$ in Pt(II), thus not being able to achieve an anionic coordination with an axial H_2O.

This conclusion can be quantified by considering the polarizability tensors of the two tetrahydrate cores, i.e. of $[M(H_2O)_4]^{2+}$ for M = Pt^{2+} and Pd^{2+}, reported in Table 3. Although the isotropic polarizability α_{iso} of this complex is virtually identical for Pt^{2+} and Pd^{2+}, there are significant differences when it comes to the anisotropy of the polarizability tensor. Within the square plane of the tetrahydrates the $\alpha_{xx} = \alpha_{yy}$ values are, again, very similar for both Pt^{2+} and Pd^{2+}, but the polarizability α_{zz} along the *z*-direction, i.e. perpendicular to this plane, is significantly larger for Pt^{2+}. Thus, the $[Pt(H_2O)_4]^{2+}$ tetrahydrate is expected to be more polarizable in the axial regions in comparison to the respective Pd^{2+} complex, which is exactly the region where anionic solvation is observed for Pt(II) in aqueous solution.

Overall, these four different ways to analyze the electronic structure yield the same qualitative picture when it comes to their solvation behavior beyond the first, tightly bonded, square-planar shell. Thus, the anionic hydration as such and also the qualitative differences between the behavior of Pt^{2+}(aq) and Pd^{2+}(aq) can be traced back in the framework of ab initio MD simulations to the electronic structure properties of the particular transition metal.

3.2.2. Metal-Water Interaction Energies in the Gas Phase. One could think that the unexpected anionic orientation found in the Pt(II) case is originated as an artifact of the electronic structure method underlying the CP-MD simulations. In order to make sure that anionic hydration is not derived from the use of a DFT method with plane waves, a number of calculations for finite solvation complexes in the gas phase have been performed using PBE/*plane waves* (*p.w.*), PBE/*Gaussian functions* (*g.f.*), and MP2/*g.f.* The *g.f.* used were of the aug-cc-pVDZ type for O and H, whereas for Pd and Pt the pseudopotentials and optimized valence basis sets (MWB pseudopotentials and cc-pVDZ basis sets) of the Stuttgart/Köln group were applied. The so-called interaction energy between the metal tetrahydrate solvation core, $[M(H_2O)_4]^{2+}$, and an axial H_2O molecule approaching the metal center in anionic and ion-dipole orientations, i.e.

$$\Delta E(d) = E([M(H_2O)_4]^{2+} \bullet H_2O) - E([M[H_2O)_4]^{2+}) - E(H_2O) \quad (1)$$

was computed in vacuum as a function of the metal-oxygen or metal-hydrogen distances, i.e. $d = d_{M-O}$ and $d_{M\text{-}H}$, using the PBE and MP2 methods. The structures of the fragments $[M(H_2O)_4]^{2+}$ and H_2O were kept frozen along the reaction path *d*. The counterpoise (CP) correction[57] to the basis set superposition error (BSSE) was applied to the raw data obtained with atom-centered gaussians, whereas the plane wave based PBE/*p.w.* calculations do not suffer from BSSE.

Figure 7 shows that both methods, PBE and MP2, yield a strong preference of the ion-dipole orientation over the repulsive anionic arrangement for both metal cations in gas phase (note the difference in energy scales of the left and right panels). In particular, both methods predict for the ion-dipole orientation well defined minima at consistent positions and attractive interaction energies for both Pd(II) and Pt(II). For the Pd(II) cation in the anionic orientation, the three methods yield curves with no minima, albeit at long distances the agreement is not good, since the PBE/*p.w.* curve shows a stronger dissociative behavior than the PBE/*g.f.* and MP2/*g.f.* curves.

In the anionic solvation case of Pt(II), shown in the lower left panel of Figure 7, there is seemingly a qualitative disagreement between the MP2 and PBE behaviors: the two PBE curves yield a very shallow minimum of about half a kcal/mol only, whereas the MP2 curve is steeply repulsive upon close approach, flat at intermediate distances, and asymptotically dissociative without displaying any metastable state. However, when it comes to assessing MP2 interaction energies, it is well documented that the full (100%) coun-

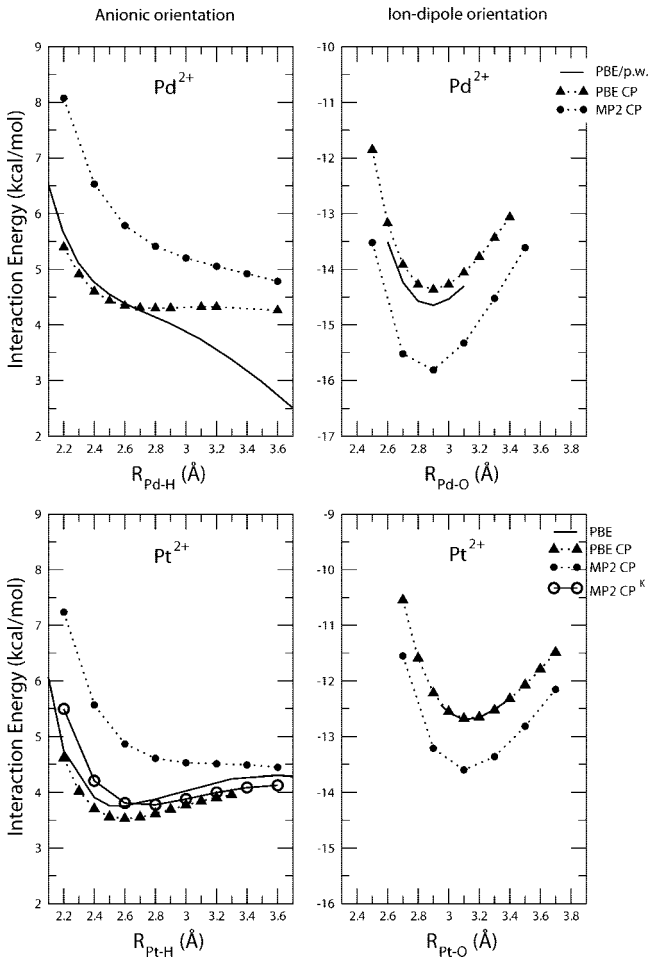

Figure 7. Interaction energies according to eq 1 between the Pd(II) (upper panels) and Pt(II) (lower panels) tetrahydrates and an additional water molecule in an axial position with anionic (left) and ion-dipole (right) orientations as a function of metal-hydrogen atom and metal-oxygen atom distances with respect to the axial H_2O molecule, respectively. The zero of energy corresponds to the isolated tetrahydrate and H_2O fragments. PBE/*g.f.* energies have been corrected for the BSSE using the (full, 100%) CP-correction,[57] whereas the PBE/*p.w.* calculations are free of BSSE. For MP2/*g.f.* energies two correction schemes have been applied: full (100%) CP-correction and, in the anionic coordination case of Pt, half (50%) CP-correction ("MP2/*g.f.* CP^K") according to ref 59.

terpoise correction overestimates the BSSE.[58] Therefore, we apply only half (50%) of the CP-correction as suggested by Kim and co-workers,[59] CP^K. It should be noted that the CP^K BSSE correction scheme is considered to be much more realiable for this type of interaction than the full CP-correction as can be judged based on previous experience on different systems, including hydration of halide anions.[59,60] The CP^K scheme yields a curve which does show a shallow minimum like the BSSE-free PBE data, whereas the full CP-correction leads to a purely repulsive interaction potential with respect to the axial water molecule in anionic orientation.

Considering all this evidence derived from PBE and MP2 calculations, the present analysis strongly suggests that the anionic orientation of the axial water molecule appears as a shallow metastable minimum for Pt(II) in the gas phase. This result is in agreement with an analogous analysis of the interaction energy between the $[Pt(NH_3)_4]^{2+}$ complex in vacuum approached by a water molecule in axial position.[17,18] Although this minimum does not account for the hydrogen pattern observed in the CP-MD simulation, in the next subsection it will be demonstrated that bulk solvation effects finally stabilize this peculiar axial water molecule in aqueous Pt(II) solutions.

3.2.3. Ion-Dipole vs Anionic Orientation in Aqueous Solution and Ligand Exchange. Once the electronic structure method employed in the CP-MD simulations has been scrutinized for the quantum mechanical interaction energy, now we study how condensed phase effects affect the two types of relative orientations of axial water molecules. The energy profile of a water molecule approaching the Pt(II) tetrahydrate along the axial direction, which is perpendicular to the metal−oxygen molecular plane of the tetrahydrate, has been built taking as geometrical coordinate the metal-water distance along that direction. In each curve, the region close to the minimum has been scanned. The reference geometries selected for these calculations (Figure 8) were extracted from a representative snapshot for the two axial coordination modes in the Pt(II) CP-MD trajectory. Specific solvent effects have been included explicitly by considering the set of three water molecules that surround the axial water molecule in the reference snapshot. Two of these additional H_2O are directly bonded to first-shell water molecules and therefore are kept fixed along the energy profile. The third H_2O is displaced with the axial water molecule, partially representing its interaction with the water network of the bulk.

Average bulk solvent effects have been introduced by means of the polarizable continuum model (PCM)[25,27] where the solvent is represented by a dielectric continuum characterized by its dielectric permittivity, ε, thus including electrostatic components of the solvation in a mean-field manner. In the case studied here, the dielectric continuum surrounds the molecular complex formed by the Pt(II) tetrahydrate and the water molecule cluster. Then, formally a semicontinuum solvation model has been adopted. This approach allows, on one hand, the definition of a part of the solvation at a molecular level for a reduced but significant number of solvent molecules and, on the other hand, satisfies the condensed medium effects by including a dielectric continuum. It is worth mentioning that although the number of explicitly included water molecules is small, the use of cavities adapted to the molecular shape allows for inclusion of certain ingredients of specific solvation.[26] In this spirit, the energies obtained with the PCM method can be used to study qualitatively the hydration of the Pt(II) tetrahydrate along a defined region, such as the axial one, the information being derived from a source independent from the CP-MD simulations.

Figure 9 shows the total PBE/*g.f.* energy as a function of the Pt−O or Pt−H distances for the two types of relative orientation of the axial water molecule illustrated in Figure 8. The energy gap between the ion-dipole and anionic orientation minima in the microsolvated representation (see Figure 9a) is 22.2 kcal/mol. When this energy gap is computed using PBE/*p.w.* the resulting value is 22.8 kcal/

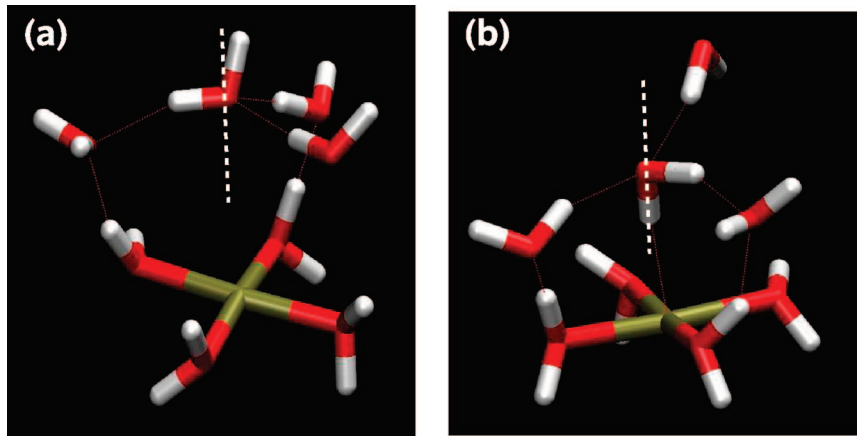

Figure 8. Structures for the water clusters, $(H_2O)[H_2O]_3$, approaching the Pt(II) tetrahydrate following a ion-dipole (left panel **a**) or anionic orientation, (right panel **b**).

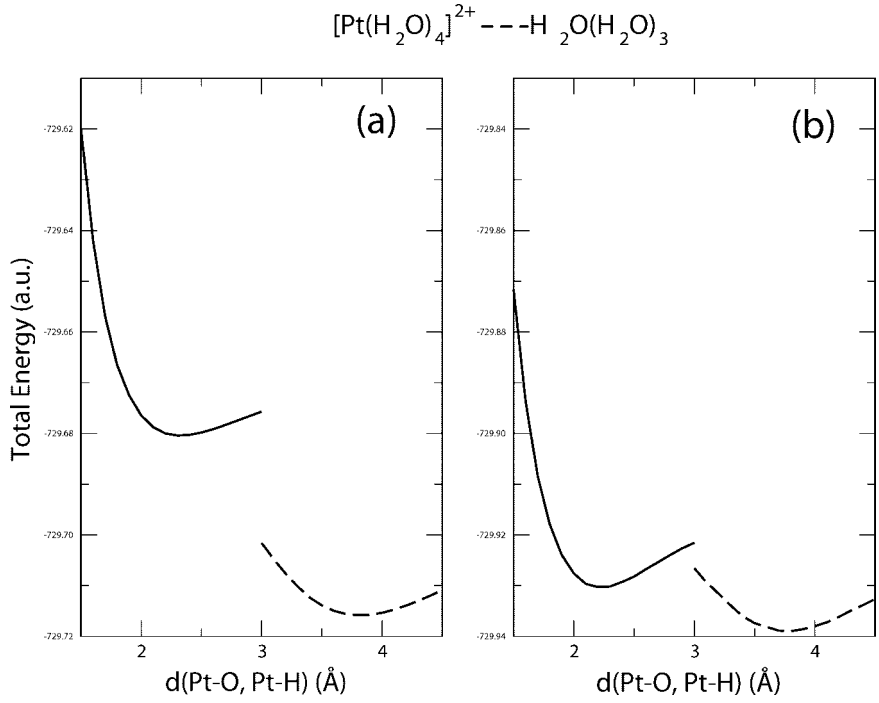

Figure 9. Interaction energies according to eq 1 between the Pt(II) tetrahydrates and an additional water molecule solvated with three water molecules in an axial position $(H_2O)[H_2O]_3$ with anionic (solid line) and ion-dipole (dashed line) orientations as a function of metal-hydrogen atom and metal-oxygen atom distances with respect to the axial H_2O molecule using the PBE/*g.f.* method. Gas phase data are reported in the left panel (a), whereas the liquid phase PCM continuum data are shown in the right panel (b).

mol. Then we can be confident that the analysis derived from these curves is not affected by different quantum mechanical ingredients than those of the CP-MD simulations. The minimum for the anionic orientation curve is defined at ca. 2.3 Å (Pt−H distance), whereas the minimum for the ion-dipole orientation is close to 3.8 Å (Pt−O distance). Interestingly, the interaction energy curve for the ion-dipole approach of one water molecule to the Pt(II) tetrahydrate (see Figure 7) shows a minimum to a much shorter Pt−O distance, ca. 3.1 Å. This indicates that the second-shell water molecules, which are strongly coordinated to the equatorial first shell, prevent a closer approach of the axial water molecule to the Pt cation. Bearing in mind that the axial partial RDFs for Pt−O show a peak at ca. 4.0 Å (see left panel of Figure 4) which corresponds to this ion-dipole orientation, it may be concluded that the main responsible of this long distance is the strong water network formed by the first and second equatorial hydration shells. The inclusion of bulk solvent effects by means of the PCM solvation model does not change significantly the position of the minima but reduces the energy gap among the minima corresponding to the two water orientations. This means that average electrostatic solute−solvent interactions preferentially favor the anionic orientation versus the ion-dipole one.

Together with intricate hydrogen bonding effects of the axial water molecule in contact with the bulk solvent as the embedding medium, which cannot be reliably modeled by any continuum approach, the anionic coordination is finally stabilized as observed in the Pt(II) solution by ab initio MD using explicit water molecules. Thus the presence of such

dynamical axial water molecules is clearly a condensed phase effect which is not expected to be observed in the gas phase. When it comes to the meso-shell found in classical MD, a similar situation has been described:[7,8] the axial hydration structure appears only when the metal cation is immersed in the solution, whereas no minimum is found for the interaction energy in the axial region in gas phase. In the present work, however, this subtle condensed phase effect is clearly worked out by comparing dynamical ab initio MD in explicit water to static ab initio approaching path calculations in both the gas phase and in implicit continuum solvent. The view supplied by the consideration of specific interactions between the axial water molecule and a reduced representation of the water network shows a significant role in the definition of the final structural arrangement by restricting particularly the closest distance approach of the ion-dipole orientation.

Pd(II) and Pt(II) square-planar coordination complexes show very different rate constants for the ligand exchange process in water. In particular, this value is about four to six *orders of magnitude* larger for Pd(II) than for Pt(II) according to refs 2, 19, and 20. Given that the exchange mechanism is thought to be associatively activated, i.e. first the incoming ligand has to attach itself to the cation before a H_2O molecule in the first shell can leave this transient complex, this different behavior can be rationalized by the presence of anionic hydration in Pt(II) and its absence in the Pd(II) case. On the one hand, the axial H_2O molecule, in spite of its short persistence, represents a sterical hindrance for the incoming ligand, which can only attack through one of the two hemispheres above and below the square plane. On the other hand, the axial H_2O polarizes the d_{z^2} electronic density of the metal toward the hemisphere it is occupying, i.e. it stablizes the solvated tetrahydrate and thus competes with the incoming ligand for the electronic density. Furthermore, when the incoming ligand is a water molecule, its preferred orientation toward the metal cation will be of the anionic type. Therefore, in order to achieve the proposed transition structure,[6,16] i.e. a trigonal-bipyramidal coordination around the metal cation, the axial H_2O has to reorient itself in order to solvate the metal properly in a cationic fashion. Since this water molecule, itself, is engaged in hydrogen bonding (see Figure 5) this implies a restructuring of its hydrogen bond network with respect to the bulk and thus an increase in the total energetic cost of the ligand exchange reaction. In the Pd(II) case the necessary rearrangement is much easier as the incoming H_2O molecule would initially coordinate through the oxygen atom, i.e. with the proper cationic orientation, implying that the exchange process is energetically less costly. Taken together, the peculiar anionic axial solvation pattern of Pt(II) versus Pd(II) would structurally, electronically, and energetically be consistent with a much less efficient ligand exchange for Pt(II) compared to Pd(II).

3.3. Transient Protolysis of Water Molecules. Based on the information extracted from the M-O RDFs, water molecules in the solution can be divided into three regions: first and second solvation shells and bulk. For each of these regions statistical distributions of O−H distances and H−O−H angles can be computed. A close examination of these parameters indicates that the structure of water molecules in the second solvation shell is already similar to that of H_2O in the bulk region so they are both considered together; details of the statistical distributions thus obtained can be found in Table 4.

Table 4. Average, Most Probable and Standard Deviation of O-H Distances ($\langle d \rangle$, d_{max}, and σ_d all in Å) and H-O-H Angles ($\langle \theta \rangle$, θ_{max}, and σ_θ all in deg) for Water Molecules in the First Hydration Shell (H_2O) and in the Bulk (H_2O) of Aqueous Pd(II) and Pt(II) Solutions

		OH distance			HOH angle		
		$\langle d \rangle$	d_{max}	σ_d	$\langle \theta \rangle$	θ_{max}	σ_θ
Pd(II):	$(H_2O)_I$	1.029	1.015	0.049	107.8	107.1	6.6
	$(H_2O)_{Bulk}$	0.999	0.993	0.031	106.0	105.7	5.7
Pt(II):	$(H_2O)_I$	1.028	1.017	0.043	109.4	109.0	6.5
	$(H_2O)_{Bulk}$	0.996	0.992	0.029	105.7	106.4	5.8

Water molecules in the first solvation shell are more strongly distorted than bulk molecules. These distortions, whose origin can be assigned to electronic charge polarization due to coordination to metal cations, are very pronounced for the O−H distances. Elongations beyond 1.2 Å suggest the onset of transient proton transfer events taking place between H_2O molecules in the first and second solvation shells. As a result of this observation the trajectories of the Pd and Pt simulations were analyzed in more detail to extract deeper insights into this phenomenon. To detect any hydronium ions, H_3O^+, the number of hydrogen atoms, n_H, within a radius of 1.20 Å of a given oxygen atom was counted.[28,29] The average lifetime of a transient hydronium ion was measured as the average period of time over the entire trajectory during which $n_H = 3$ continuously. To complete the structural characterization of these H_3O^+ ions, also the degree of pyramidalization[61] was computed along the trajectory.

In the Pd case, 23 events consisting of first shell H_2O molecules transferring a proton to a second shell H_2O were found, whereas for Pt only 9 such events were observed. The pyramidalization degree of the H_3O^+ ion fluctuates between about 5 and 25° in both simulations. Effective protolysis of H_2O in the first hydration shell would imply translocation of the dissociated proton further away from the second solvation shell[30,37] and its subsequent diffusion through the bulk.[33] In all cases observed, however, the proton bonded back to the first-shell water molecule, i.e. the nascent hydronium did not detach from the solvation complex and thus did not undergo Grotthuss structural diffusion[28,31] so that no proton transport was observed.[31,32] Thus, we observed *spontaneous cation-induced transient protolysis* in these aqueous Pt(II) and Pd(II) solutions. Although these results clearly do not allow for a quantitative prediction of the pK_a values for Pd(II) and Pt(II) tetrahydrates, they do agree qualitatively with experimental measures of the acidic character of these two aqua ions the Pd(II) hydrate being slightly more acidic than the Pt(II) one (with measured pK_a values of 2.3 for Pd(II)[1] and 2.5 for Pt(II)[2]). It is mentioned in passing that no correlation between transient protolysis events and anionic axial hydration events was found.

What are the implications of this phenomenon on the modeling of such transition metal solutions with the aim to extend the length and time scales beyond what is accessible by ab initio MD? The average lifetime of H_3O^+ in the second solvation shell was 7.4 fs in the Pd solution and 4.9 fs in the Pt case. Thus, the tetrahydrated cations $[M(H_2O)_4]^{2+}$ transformed spontaneously into the $[M(H_2O)_3(OH)]^+$ aquo complexes during about 1.5% and 0.4% of the total simulation time for Pd and Pt, respectively. Water molecules directly coordinated to the metal cation suffer from polarization and partial electron transfer toward the metal and thus exhibit a stronger acid behavior than in the bulk. Thus, the tetrahydrate complexes experience a certain number of hydrolysis events, during which the metal bears a lower effective charge. In order to achieve such a fine description of the system, which might be necessary in order to deal with ligand exchange e.g. in cisplatin-like compounds, the solvated aqua ion normally represented by $[M(H_2O)_4]^{2+}$ should be considered as the more complex *dynamical entity* $[M(H_2O)_4]^{2+} \cdot (H_2O)_m \leftrightarrow [M(H_2O)_3(OH)]^+ \cdot [(H_3O)(H_2O)_{m-1}]^+$. This level of modeling might be relevant in order to build more reliable intermolecular potentials to be used in classical MD simulations of hydrates of transition metal cations, possibly following similar strategies as those employed previously for neat liquid water.[62−64]

4. Concluding Remarks and Outlook

The structure, energetics, and electronic structure of the hydration pattern of Pd(II) and Pt(II) cations in bulk water has been studied using Car-Parrinello ab initio MD at ambient conditions. In addition to the well-established general feature of a rather rigid square-planar first solvation shell, $[M(H_2O)_4]^{2+}$, two important special features of these solvated transition metal complexes have been analyzed in detail: "anionic solvation" in the axial regions and "transient protolysis" in the first solvation shell. In the case of the aqueous Pt(II) solution, an additional fifth water molecule could be identified in the *axial regions* being weakly coordinated to the metal cation via its *hydrogen atom*, which is the generic orientation of first-shell solvent water around *anions*. These features could only be unravelled using angle-resolved radial distribution functions; they cannot be resolved by standard spherically-averaged radial distribution functions. Electronic structure analyses suggest that this contact can be viewed as a weak hydrogen bonding interaction established between the d_{z^2} orbital of the metal and one hydrogen atom of the water molecule as a result of polarization effects. In contrast, axial water molecules at a second-shell distance from Pd^{2+} are characterized by a normal cationic orientation dictated by the dipole moment vector of H_2O. The qualitative difference in axial hydration between Pd(II) and Pt(II) may well be connected to the lower polarizability of the Pd(II) compared to the Pt(II) tetrahydrate along the *axial* direction. Detailed analyses uncover that the stabilization of a fifth water molecule in an axial position is a condensed phase effect that is absent in microsolvated complexes in the gas phase. Additionally, static quantum-chemical calculations of interaction energies as a function of distance between the square-planar tetrahydrates and a fifth water molecule using the Polarizable Continuum Model approach support the idea that anionic hydration is indeed a direct consequence of the presence of the solvent. Axial solvation refines the previously proposed meso-shell concept[7,8] uncovered in classical MD simulations of these transition metals in solution, where the solvation is symmetric with respect to the square plane, better defined, and cationic for both species.

This peculiar axial solvation pattern also impacts the first-shell ligand exchange of square-planar Pd(II) and Pt(II) complexes in water, which is several orders of magnitude faster for Pd(II) compared to Pt(II). The accepted mechanism for these water exchange reactions is associative and includes a transition state with a trigonal-bipyramidal structure with all oxygens pointing toward the metal, which involves a relevant participation of the regions above and below the metal-oxygen plane before its formation. The main observable structural difference between Pd(II) and Pt(II) aqua ions is an anionic axial solvation in the case of Pt, whereas a less pronounced and cationic solvation is seen for Pd above and below the metal-oxgyen plane. It is thus conceivable that the *anionic* arrangement in the case of Pt is unfavorable for associative ligand exchange via a 5-fold cationically coordinated intermediate, whereas the *cationic* orientation in Pd favors that process. This might have further ramifications for ligand exchange rates of novel cisplatin-based drugs, currently investigated within our collaboration.

Water molecules in the first hydration shell of Pd(II) and Pt(II) show also an enhanced "acidity" compared to H_2O in the bulk due to polarization and charge transfer effects with the metal cation favoring cation-induced transient protolysis in the first shell. The underlying proton transfer from first-shell water molecules into the second shell has been analyzed and found to be more pronounced for Pt in qualitative agreement with experimental pK_a differences. Although hydrolysis phenomena have been characterized previously for several *trivalent* cations, such as Al(III)[34−37] as well as Cr(III) and Fe(III),[37] these aqua ions are generally well coordinated, whereas in the case of divalent Pd(II) and Pt(II) only four H_2O in a very open square-planar coordination stabilize the +2 charge at the center. This seems to allow for protolysis in the neighborhood of these divalent cations, although to a much lesser extent compared to trivalent cations. To take into account this feature together with proper axial solvation is a challenge to future force field based modeling of Pt(II) metals in aqueous solution and, in particular, of cisplatin-based anticancer drugs.

Acknowledgment. We thank Barcelona Supercomputer Center for computer time, technical expertise, and assistance. Drs. B. Meyer and N. Nair (Bochum) are acknowledged for helpful discussions. Spanish DGICYT is acknowledged for financial support (CTQ2005-3657). E.C.B. acknowledges the Spanish Ministerio de Educacion y Ciencia for a doctoral fellowship and financial support of her research visits in Bochum. D.M. is grateful for partial financial support provided by Fonds der Chemischen Industrie (FCI).

References

(1) Nabivanets, B. I.; Kalabina, L. V. *Russ. J. Inorg. Chem.* **1970**, *15*, 818.

(2) Elding, L. I. *Inorg. Chim. Acta* **1976**, *20*, 65.

(3) Hellquist, B.; Bengtsson, L. A.; Holmberg, B.; Hedman, B.; Persson, I.; Elding, L. I. *Acta Chem. Scand.* **1991**, *45*, 449–455.

(4) Ayala, R.; Sánchez Marcos, E.; Díaz-Moreno, S.; Armando Solé, V.; Muñoz-Páez, A. *J. Phys. Chem. B* **2001**, *105*, 7588–7593.

(5) Purans, J.; Fourest, B.; Cannes, C.; Sladkov, V.; David, F.; Venault, L.; Lecomte, M. *J. Phys. Chem. B* **2005**, *109*, 11074–11082.

(6) Deeth, R. J.; Elding, L. I. *Inorg. Chem.* **1996**, *35*, 5019–5026.

(7) Martínez, J. M.; Torrico, F.; Pappalardo, R. R.; Sánchez Marcos, E. *J. Phys. Chem. B* **2004**, *108*, 15851–15855.

(8) Torrico, F.; Pappalardo, R. R.; Marcos, E. S.; Martínez, J. M. *Theor. Chem. Acc.* **2006**, *115*, 196–203.

(9) Shah, S.; Hofer, T. S.; Fatmi, M. Q.; Randolf, B. R.; Rode, B. M. *Chem. Phys. Lett.* **2006**, *426*, 301–305.

(10) Hofer, T. S.; Randolf, B. R.; Shah, S.; Rode, B. M.; Persson, I. *Chem. Phys. Lett.* **2007**, *445*, 193–197.

(11) Richens, D. T. *The Chemistry of Aqua Ions*; John Wiley and Sons: 1977.

(12) Frank, H. S.; Evans, M. W. *J. Chem. Phys.* **1945**, *13*, 507–532.

(13) Caminiti, R.; Carbone, M.; Sadun, C. *J. Mol. Liq.* **1998**, *75*, 149–158.

(14) Lopes, J. F.; de A. Menezes, V. S.; Duarte, H. A.; Rocha, W. R.; de Almeida, W. B.; Dos Santos, H. F. *J. Phys. Chem. B* **2006**, *110*, 12047–12054.

(15) Carloni, P.; Sprik, M.; Andreoni, W. *J. Phys. Chem. B* **2000**, *104*, 823–835.

(16) Song, T.; Hu, P. *J. Chem. Phys.* **2006**, *125*, 091101-1-3.

(17) Kozelka, J.; Bergès, J.; Attias, R.; Fraitag, J. *Angew. Chem., Int. Ed.* **2000**, *39*, 198–201.

(18) Bergès, J.; Caillet, J.; Langlet, J.; Kozelka, J. *Chem. Phys. Lett.* **2001**, *344*, 573–577.

(19) Helm, L.; Merbach, A. E. *Chem. Rev.* **2005**, *105*, 1923–1959.

(20) Rotzinger, F. P. *Chem. Rev.* **2005**, *105*, 2003–2037.

(21) Gill, D. S. In *Platinum Coordination Complexes in Cancer Chemotherapy*; Hacker et al. Eds.; Martinus Nijhoff Publishing: 1984; pp 267−278.

(22) Car, R.; Parrinello, M. *Phys. Rev. Lett.* **1985**, *55*, 2471–2474.

(23) Marx, D.; Hutter, J. Ab Initio Molecular Dynamics: Theory and ImplementationIn *Modern Methods and Algorithms of Quantum Chemistry*; Grotendorst, J., Ed.; NIC, FZ Jülich: 2000. See www.theochem.rub.de/go/cprev.html (accessed October 2008).

(24) Beret, E. C.; Pappalardo, R. R.; Doltsinis, N. L.; Marx, D.; Sánchez Marcos, E. *ChemPhysChem* **2008**, *9*, 237–240.

(25) Tomasi, J.; Persico, M. *Chem. Rev.* **1994**, *94*, 2027.

(26) Martínez, J. M.; Pappalardo, R. R.; Sánchez Marcos, E.; Mennucci, B.; Tomasi, J. *J. Phys. Chem. B* **2002**, *106*, 1118–1123.

(27) Tomasi, J.; Mennucci, B.; Cammi, R. *Chem. Rev.* **2005**, *105*, 2999–3094.

(28) Tuckerman, M.; Laasonen, K.; Sprik, M.; Parrinello, M. *J. Chem. Phys.* **1995**, *103*, 150–161.

(29) Trout, B. L.; Parrinello, M. *J. Phys. Chem. B* **1999**, *103*, 7340–7345.

(30) Geissler, P. L.; Dellago, C.; Chandler, D.; Hutter, J.; Parrinello, M. *Science* **2001**, *291*, 2121.

(31) Tuckerman, M. E.; Chandra, A.; Marx, D. *Acc. Chem. Res.* **2006**, *39*, 151–158.

(32) Chandra, A.; Tuckerman, M. E.; Marx, D. *Phys. Rev. Lett.* **2007**, *99*, 145901-1-4.

(33) Marx, D. *ChemPhysChem* **2006**, *7*, 1848–1870. See addendum: *ChemPhysChem* **2007**, *8*, 209-210.

(34) Sillanpää, A. J.; Päivärinta, J. T.; Hotokka, M. J.; Rosenholm, J. B.; Laasonen, K. E. *J. Phys. Chem. A* **2001**, *105*, 10111–10122.

(35) Ikeda, T.; Hirata, M.; Kimura, T. *J. Chem. Phys.* **2003**, *119*, 12386–12392.

(36) Swaddle, T. W.; Rosenqvist, J.; Yu, P.; Bylaska, E.; Phillips, B. L.; Casey, W. H. *Science* **2005**, *308*, 1450–1453.

(37) Coskuner, O.; Jarvis, E. A. A.; Allison, T. C. *Angew. Chem., Int. Ed* **2007**, *46*, 7853–7855.

(38) Hutter, J. et al. *CPMD V.3.11*; Copyright IBM Corp. 1990−2006, Copyright MPI für Festkörperforschung Stuttgart 1997−2001.

(39) Perdew, J. P.; Burke, K.; Ernzerhof, M. *Phys. Rev. Lett.* **1996**, *77*, 3865–3868.

(40) Perdew, J. P.; Burke, K.; Ernzerhof, M. *Phys. Rev. Lett.* **1997**, *78*, 1396.

(41) Vanderbilt, D. *Phys. Rev. B* **1985**, *32*, 8412–8415.

(42) Fernández-Serra, M. V.; Artacho, E. *J. Chem. Phys.* **2004**, *121*, 11136–11144.

(43) Goedecker, S.; Teter, M.; Hutter, J. *Phys. Rev. B: Condens. Matter* **1996**, *54*, 1703–1710.

(44) Andrae, D.; Haeussermann, U.; Dolg, M.; Stoll, H.; Preuss, H. *Theor. Chim. Acta* **1990**, *77*, 123–141.

(45) Frisch, M. J.; Trucks, G. W.; Schlegel, H. B.; Scuseria, G. E.; Robb, M. A.; Cheeseman, J. R.; Montgomery, J. A., Jr.; Vreven, T.; Kudin, K. N.; Burant, J. C.; Millam, J. M.; Iyengar, S. S.; Tomasi, J.; Barone, V.; Mennucci, B.; Cossi, M.; Scalmani, G.; Rega, N.; Petersson, G. A.; Nakatsuji, H.; Hada, M.; Ehara, M.; Toyota, K.; Fukuda, R.; Hasegawa, J.; Ishida, M.; Nakajima, T.; Honda, Y.; Kitao O.; Nakai, H.; Klene, M.; Li, X.; Knox, J. E.; Hratchian, H. P.; Cross, J. B.; Bakken, V.; Adamo, C.; Jaramillo, J.; Gomperts, R.; Stratmann, R. E.; Yazyev, O.; Austin, A. J.; Cammi, R.; Pomelli, C.; Ochterski, J. W.; Ayala, P. Y.; Morokuma, K.; Voth, G. A.; Salvador, P.; Dannenberg, J. J.; Zakrzewski, V. G.; Dapprich, S.; Daniels, A. D.; Strain, M. C.; Farkas, O.; Malick, D. K.; Rabuck, A. D.; Raghavachari, K.; Foresman, J. B.; Ortiz, J. V.; Cui, Q.; Baboul, A. G.; Clifford, S.; Cioslowski, J.; Stefanov, B. B.; Liu, G.; Liashenko, A.; Piskorz, P.; Komaromi, I.; Martin, R. L.; Fox, D. J.; Keith, T.; Al-Laham, M. A.; Peng, C. Y.; Nanayakkara, A.; Challacombe, M.; Gill, P. M. W.; Johnson, B.; Chen, W.; Wong, M. W.; Gonzalez, C.; Pople, J. A. *Gaussian 03, Revision C.02*; Gaussian, Inc.: Wallingford, CT, 2004.

(46) Dunning, T. H. J. *J. Chem. Phys.* **1989**, *90*, 1007–1023.

(47) Mennucci, B.; Tomasi, J. *J. Chem. Phys.* **1997**, *106*, 5151.

(48) Cancès, M. T.; Menucci, B.; Tomasi, J. *J. Chem. Phys.* **1997**, *107*, 3032–3041.

(49) Mennucci, B.; Cances, E.; Tomasi, J. *J. Phys. Chem. B* **1997**, *101*, 10506.

(50) Tomasi, J.; Mennucci, B.; Cances, E. *J. Mol. Struct. (Theochem)* **1999**, *464*, 211.

(51) Rappe, A. K.; Casewit, C. J.; Colwell, K. S.; Goddard, W. A., III; Skiff, W. M. *J. Am. Chem. Soc.* **1992**, *114*, 10024.

(52) Serr, A.; Netz, R. R. *Int. J. Quantum Chem.* **2006**, *106*, 2960–2974.

(53) Peterson, K. A.; Figgen, D.; Dolg, M.; Stoll, H. *J. Chem. Phys.* **2007**, *126*, 124101.

(54) Heinzinger, K.; Vogel, P. C. *Z. Naturforsch. A* **1974**, *29*, 1164–1171.

(55) Ohtaki, H.; Radnai, T. *Chem. Rev.* **1993**, *93*, 1157–1204.

(56) Marzari, N.; Vanderbilt, D. *Phys. Rev. B* **1997**, *56*, 12847.

(57) Boys, S. F.; Bernardi, F. *Mol. Phys.* **1970**, *19*, 553–566.

(58) Rayon, V. M.; Sordo, J. A. *J. Phys. Chem. A* **1997**, *101*, 7414–7419.

(59) Kim, K. S.; Tarakeshwar, P.; Lee, J. Y. *Chem. Rev.* **2000**, *100*, 4145–4185.

(60) Singh, N. J.; Olleta, A. C.; Kumar, A.; Park, M.; Yi, H.; Bandyopadhyay, I.; Lee, H. M.; Tarakeshwar, P.; Kim, K. S. *Theor. Chem. Acc.* **2006**, *115*, 127–135.

(61) Haddon, R. C. *J. Am. Chem. Soc.* **1990**, *112*, 3385–3389.

(62) Halley, J. W.; Rustad, J. R.; Rahman, A. *J. Chem. Phys.* **1993**, *98*, 4110–4119.

(63) Mahadevan, T. S.; Garofalini, S. H. *J. Phys. Chem. B* **2007**, *111*, 8919–8927.

(64) Izvekov, S.; Parrinello, M.; Burnham, C. J.; Voth, G. A. *J. Chem. Phys.* **2004**, *120*, 10896–10913.

CT800010Q